Pergamon

Int. J. Heat Mass Transfer. Vol. 39, No. 16, pp. 3483–3496, 1996

0017-9310/96 $15.00+0.00

0017-9310(95)00356-8

New low-Reynolds-number k–ε model including damping effect due to buoyancy in a stratified flow field

S. MURAKAMI and S. KATO

Institute of Industrial Science, University of Tokyo, 22-1, Roppongi 7-chome, Minato-ku, Tokyo 106, Japan

T. CHIKAMOTO

Nikken Sekkei Ltd, 2-1-3, Koraku, Bunkyo-ku, Tokyo 112, Japan

D. LAURENCE

Electricité de France, 6, quai Watier, B.P. 49, 78401 Chatou Cedex, France

and

D. BLAY

Laboratoire d'Etudes Thermiques, ENSMA, B.P. 109, F-86960, Futuroscope Cedex, France

(*Received* 12 *September* 1994 *and in final form* 18 *August* 1995)

Abstract—A new k–ε model which includes damping effect on vertical turbulent transport due to thermal stratification is proposed. The proposed model was tested by application to two kinds of two-dimensional thermally stratified flow fields. One is a high-Reynolds-number open channel flow, and the other is a low-Reynolds-number flowfield within an enclosure. The new model also includes low-Reynolds-number treatment which is effective not only in the vicinity of the wall, but also apart from the wall. With the aid of this new low-Reynolds-number treatment, the proposed k–ε model becomes applicable to a flowfield which includes both turbulent area and pseudo-laminar area caused by thermal stratification. The agreement between the results given from the new k–ε model and the experimental results was rather good.

1. INTRODUCTION

Stable stratification is often observed in many kinds of flow. The flowfield within an enclosed space, e.g. room airflow with air-conditioning, is often thermally stratified. One typical example is the flowfield in a glass-covered atrium with large ceiling height. Sunshine penetrates its glazed roof and often leaves the flowfield thermally stratified and roughly laminar. This stable stratification suppresses the vertical flux of heat and momentum, i.e. the turbulence flux of momentum and heat in the vertical direction, ($-\overline{u_1u_3}$, $-\overline{u_2u_3}$, $-\overline{u_3^2}$, $-\overline{u_3\theta}$), and also decreases the turbulence intensity (k) of the flowfield.

The standard k–ε model [1] has been widely used and has yielded reasonable solutions not only in isothermal, but also in non-isothermal flowfields. However, the k–ε model does not always lead to accurate and stable results in the simulation of a stably stratified flowfield, because the k–ε model was developed on the basis of isotropic EVM (eddy viscosity model) and EDM (eddy diffusivity model). Since this model is very simple and popular, it would be very useful and practical if modifications to the standard k–ε EVM could overcome the existing difficulties in analyzing thermally stratified flow fields.

It has been clarified that more elaborate turbulence models such as DSM (differential stress model) and ASM (algebraic stress model) can predict non-isothermal flowfield accurately even when non-isotropic effect is very large [2]. These models solve Reynolds stress transport equations and heat flux transport equations directly without using the isotropic EVM and EDM. However, the number of equations to be solved is increased and much CPU time is needed in the DSM or ASM. In this study, the application of these more elaborate models was not tried. The purpose of this study is to propose a simple model which is based on the EVM, yet remedies the shortcomings of the EVM and which also can estimate the properties of a flowfield with stable stratification easily and accurately.

In a stably stratified flow, the transport of turbulence in the vertical direction is suppressed greatly

NOMENCLATURE

C_μ, $C_{\varepsilon 1}$, $C_{\varepsilon 2}$ turbulence model constants
C_{BV1}, C_{BV2}, C_{BV3}, $C_{B\theta 1}$, $C_{B\theta 2}$, $C_{B\theta 3}$ turbulence model constants of damping functions
C_1, C_2, $C_{\theta 1}$, $C_{\theta 2}$, $C_{\theta 3}$ model constants of ASM
D_{ij} diffusion term of $\overline{u_i u_j}$
$D_{i\theta}$ diffusion term of $\overline{u_i\theta}$
f_{BV} damping function for $\overline{u_i u_j}$ due to buoyancy
$f_{B\theta}$ damping function for $\overline{u_i\theta}$ due to buoyancy
f_μ model function due to low-Reynolds-number effect of eddy viscosity
f_1, f_2 model function due to low-Reynolds-number effect in ε equation
G_k buoyancy production term of k $(-g_i\beta\overline{u_i\theta})$
G_{ij} buoyancy production of $\overline{u_i u_j}$ $(-g_i\beta\overline{u_j\theta}-g_j\beta\overline{u_i\theta})$
$G_{i\theta}$ buoyancy production of $\overline{u_i\theta}$ $(-g_i\beta\overline{\theta^2})$
g_i gravity acceleration in i direction $(g_3 = -9.8)$
k turbulent energy
l turbulent length scale $(k^{3/2}/\varepsilon)$
P_{ij} shear production term of $\overline{u_i u_j}$ $(-(\overline{u_j u_k}\,(\partial\overline{U}_i/\partial x_k)+\overline{u_i u_k}\,(\overline{U}_j/\partial x_k)))$
$P_{i\theta(1)}$ production term of $u_i\theta$ by temperature gradient $(-\overline{u_i u_k}\,(\partial\overline{\Theta}/\partial x_k))$
$P_{i\theta(2)}$ production term of $\overline{u_i\theta}$ by velocity gradient $(-\overline{u_k\theta}\,(\partial\overline{U}_i/\partial x_k))$
P_k shear production term of k $(-\overline{u_i u_j}\cdot\partial\overline{U}_i/\partial x_j)$
P_θ production term of $\overline{\theta^2}$ $(-2\overline{u_k\theta}\,(\partial\overline{\Theta}/\partial x_k))$
R ratio of time scale of temperature fluctuation and that of velocity fluctuation $((\overline{\theta^2}/2\varepsilon_\theta)/(k/\varepsilon))$
Rt turbulent Reynolds number $(k^2/(\nu\varepsilon))$
$\overline{U}_i$ mean velocity in i-direction ($i = 1, 2$: horizontal direction, $i = 3$: vertical direction)
u_i fluctuating velocity in i-direction
u_ε Kolmogorov velocity scale $((\nu\varepsilon)^{1/4})$
$-\overline{u_i u_j}$ Reynolds stress
$-\overline{u_i\theta}$ turbulent heat flux
y length from wall surface
y^+ non-dimensional length from wall surface $(u^*\cdot y/\nu)$
u^* friction velocity.

Greek symbols
β coefficient of volume expansion
δ_{ij} Kronecker delta
ε dissipation rate of turbulence energy k
ε_{ij} dissipation term of $\overline{u_i u_j}$
$\varepsilon_{i\theta}$ dissipation term of $\overline{u_i\theta}$
ε_θ dissipation term of $\overline{\theta^2}/2$
η Kolmogorov length scale $(\nu^{3/4}/\varepsilon^{1/4})$
$\overline{\Theta}$ mean temperature
θ temperatue fluctuation
ν_t eddy viscosity
ν kinematic viscosity
ρ density
σ_k, σ_ε model constants in turbulent diffusion terms of k-ε model
σ_θ turbulent Prandtl number
ϕ_{ij} pressure-strain correlation term $(\overline{(p/\rho)\,((\partial u_j/\partial x_i)+(\partial u_i/\partial x_j))})$
$\phi_{i\theta}$ pressure-temperature gradient correlation term $(\overline{(p/\rho)\,(\partial\theta/\partial x_i)})$.

Subscripts
i, j 1, 2 and 3 denote x-, y- and z-directions, respectively.

in spite of the large mean velocity gradient in the vertical direction. This damping effect by buoyancy in the gravitational direction, i.e. the vertical damping effect, plays an important role in the flow characteristics. It is well-known that the standard k–ε model cannot express this effect well. Therefore, a new k–ε model which includes the damping effect on the vertical turbulence transport due to the thermal stratification is proposed.

In a stably stratified flow, the flow sometimes becomes pseudo-laminar in which the turbulence intensity is negligibly small because of the damping effect by buoyancy. Hereby a low-Reynolds-number effect is to be considered in the new k–ε model.

When the flow becomes laminar, such as in an area in the vicinity of the wall, the standard k–ε model which uses the so-called wall functions does not work well. The wall functions bridge the turbulent region and the wall surface. In order to predict the laminarization correctly in the vicinity of the wall, many types of low-Reynolds-number k–ε models have been proposed since Jones and Launder [3].

In most of the previous studies, these low-Reynolds-number k–ε models have been used successfully to predict a flow with the laminar region near the wall. However, in predicting laminar flow away from the wall caused by stable stratification, these existing low-Reynolds-number k–ε models do not work well since they only use the non-dimensionalized distance from the wall for the near wall treatment. Thus, they should be modified.

In this paper, a new low-Reynolds-number model

is proposed in addition to new model functions of buoyancy damping. With the aid of this low-Reynolds-number treatment, this new k–ε model is applicable to a pseudo-laminar flowfield, even outside the vicinity of the wall.

2. DEVELOPMENT OF k–ε EVM FOR INCLUDING DAMPING EFFECT DUE TO STABLE STRATIFICATION

There have been many studies on developing turbulence models to predict stable stratification [4–7].

However, from the viewpoint of practical application, these models are not simple enough, and their application to complex flows, e.g. flows in rooms, is not easy.

The design concept of the new model is intended to be simple, thus two model functions f_{BV}, $f_{B\theta}$ are introduced into the EVM and the EDM to reflect the buoyancy damping [cf. equations (1), (2) and note]. With this small modification, we have succeeded in introducing the mechanism of the vertical damping effect by buoyancy into the EVM and EDM, and the decrease of the vertical flux of heat and momentum ($-\overline{u_1u_3}$, $-\overline{u_2u_3}$, $-\overline{u_3^2}$, $-\overline{u_3\theta}$) is well reproduced in stratified flow fields.

$$-\overline{u_iu_j} = C_\mu f_\mu f_{BV}\frac{k^2}{\varepsilon}\left(\frac{\partial \overline{U_i}}{\partial x_j}+\frac{\partial \overline{U_j}}{\partial x_i}\right)-\tfrac{2}{3}k\delta_{ij} \tag{1}$$

$$-\overline{u_i\theta} = \frac{1}{\sigma_\theta}C_\mu f_\mu f_{B\theta}\frac{k^2}{\varepsilon}\frac{\partial \overline{\Theta}}{\partial x_i}. \tag{2}$$

Overbar ($\bar{}$) denotes the ensemble-mean value. C_μ is the model constant ($C_\mu = 0.09$. This value is rather empirically tuned so that the correspondences between the predictions and observed characteristics should be satisfactory for various forced convection flows. However, with this value the standard model has been widely used and has yielded a reasonable solution for forced and even natural convection flow. Therefore, this standard value is adopted, and this leads to minimum modification on the standard model for developing a new model.)

f_μ is the model function to account for the near-wall and the low-Reynolds-number effect. When the flow becomes turbulent (with high-Reynolds-number), $f_\mu = 1$.

Each subscript B, V and θ in f_{BV} and $f_{B\theta}$ means buoyancy, velocity and temperature, respectively.

2.1. *Model function* f_{BV} *for damping* $\overline{u_iu_j}$

The stably stratified shear flow is roughly two-dimensional. Here coordinate x_1 indicates streamwise, x_2 spanwise and x_3 vertically upwards, respectively. In a stably stratified flow, the following can be assumed; (1) $|\overline{U_3}| \ll |\overline{U_1}|$, (2) $\overline{U_1}$ and $\overline{\Theta}$ vary greatly in the vertical direction, but little in the horizontal direction, and (3) $\partial\overline{\Theta}/\partial x_3$ has a large positive value. In this stably stratified flow, shear stresses $-\overline{u_1u_3}$ and $-\overline{u_2u_3}$ (and $-\overline{u_3\theta}$) have the most important roles in determining the flow features. Therefore, when the model is designed, it is intended that shear stresses $-\overline{u_1u_3}$ and $-\overline{u_2u_3}$ are very accurately predicted. Thus, as shown in equations (3)–(8), damping function f_{BV} modifies only these shear stresses, $-\overline{u_1u_3}$ and $-\overline{u_2u_3}$, in the application to the three-dimensional flow field.

$$-\overline{u_1^2} = 2\nu_t\frac{\partial \overline{U_1}}{\partial x_1}-\tfrac{2}{3}k \tag{3}$$

$$-\overline{u_2^2} = 2\nu_t\frac{\partial \overline{U_2}}{\partial x_2}-\tfrac{2}{3}k \tag{4}$$

$$-\overline{u_3^2} = 2\nu_t\frac{\partial \overline{U_3}}{\partial x_3}-\tfrac{2}{3}k \tag{5}$$

$$-\overline{u_1u_2} = \nu_t\left(\frac{\partial \overline{U_1}}{\partial x_2}+\frac{\partial \overline{U_2}}{\partial x_1}\right) \tag{6}$$

$$-\overline{u_1u_3} = \nu_t f_{BV}\left(\frac{\partial \overline{U_1}}{\partial x_3}+\frac{\partial \overline{U_3}}{\partial x_1}\right) \tag{7}$$

$$-\overline{u_2u_3} = \nu_t f_{BV}\left(\frac{\partial \overline{U_2}}{\partial x_3}+\frac{\partial \overline{U_3}}{\partial x_2}\right). \tag{8}$$

Here eddy viscosity ν_t is defined as follows:

$$\nu_t = C_\mu k^2/\varepsilon.$$

For considering the low-Reynolds-number effect, the model function f_μ is multiplied to eddy viscosity [cf. equation (53)].

f_{BV} is derived by approximating the Reynolds stress transport equation (9).

$$\frac{D\overline{u_iu_j}}{Dt} = P_{ij}+G_{ij}+\Phi_{ij}+D_{ij}-\varepsilon_{ij}. \tag{9}$$

For modeling the pressure–strain term Φ_{ij}, the Rotta's model for the slow term and the IPM (isotropitization of production model) for the rapid term are adopted, respectively. Then, equation (10) is given as

$$\Phi_{ij} = -C_1\frac{\varepsilon}{k}(\overline{u_iu_j}-\tfrac{2}{3}k\delta_{ij})-C_2(P_{ij}-\tfrac{2}{3}P_k\delta_{ij}) - C_2(G_{ij}-\tfrac{2}{3}G_k\delta_{ij}). \tag{10}$$

In equation (10), model constants are given following Launder [9]:

$$C_1 = 1.8, C_2 = 0.6.$$

In equation (9), dissipative motion is assumed to be isotropic.

$$\varepsilon_{ij} = \tfrac{2}{3}\varepsilon\delta_{ij}. \tag{11}$$

By neglecting the convection and diffusion terms and also assuming local equilibrium ($\varepsilon = P_k+G_k$) in equation (9), the so-called WET model by Launder [8] is derived [equation (12)].

$$-\overline{u_iu_j} = -C'\frac{k}{\varepsilon}\{(P_{ij}-\tfrac{2}{3}P_k\delta_{ij})+(G_{ij}-\tfrac{2}{3}G_k\delta_{ij})\} -\tfrac{2}{3}k\delta_{ij}. \quad (12)$$

Equation (12) is re-expressed as follows:

$$-\overline{u_iu_j} = C'\frac{k}{\varepsilon}\left(\overline{u_ju_k}\frac{\partial\overline{U_i}}{\partial x_k}+\overline{u_iu_k}\frac{\partial\overline{U_j}}{\partial x_k}-\tfrac{2}{3}\overline{u_ku_l}\frac{\partial\overline{U_l}}{\partial x_k}\delta_{ij}\right) +C'\frac{k}{\varepsilon}(g_i\beta\overline{u_j\theta}+g_j\beta\overline{u_i\theta}-\tfrac{2}{3}g_k\beta\overline{u_k\theta}\delta_{ij}) -\tfrac{2}{3}k\delta_{ij}. \quad (13)$$

Here $C' = (1-C_2)/C_1 = 0.22$. Shear stress $(-\overline{u_1u_3})$ is represented by equation (14).

$$-\overline{u_1u_3} = C'\frac{k}{\varepsilon}\left(\overline{u_1u_3}\frac{\partial\overline{U_1}}{\partial x_1}+\overline{u_2u_3}\frac{\partial\overline{U_1}}{\partial x_2}+\overline{u_3^2}\frac{\partial\overline{U_1}}{\partial x_3} +\overline{u_1^2}\frac{\partial\overline{U_3}}{\partial x_1}+\overline{u_1u_2}\frac{\partial\overline{U_3}}{\partial x_2}+\overline{u_1u_3}\frac{\partial\overline{U_3}}{\partial x_3}\right) +C'\frac{k}{\varepsilon}g_3\beta\overline{u_1\theta}. \quad (14)$$

Considering the flow property with stably stratified flow in an enclosure,

$$\frac{\partial}{\partial x_3} \gg \frac{\partial}{\partial x_1} \sim \frac{\partial}{\partial x_2}$$

can be assumed. Also

$$\overline{U_3}, \frac{\partial\overline{U_3}}{\partial x_3}$$

can be assumed to be negligibly small here. Thus equation (14) is simply expressed as equation (15).

$$-\overline{u_1u_3} \simeq C'\frac{k}{\varepsilon}\overline{u_3^2}\frac{\partial\overline{U_1}}{\partial x_3}. \quad (15)$$

Normal stress in the vertical direction $\overline{u_3^2}$ in equation (15) is given as equation (16).

$$-\overline{u_3^2} = C'\frac{k}{\varepsilon}\left(2\overline{u_1u_3}\frac{\partial\overline{U_3}}{\partial x_1}+2\overline{u_2u_3}\frac{\partial\overline{U_3}}{\partial x_2} +2\overline{u_3^2}\frac{\partial\overline{U_3}}{\partial x_3}+\tfrac{2}{3}P_k\right)+\tfrac{4}{3}C'\frac{k}{\varepsilon}g_3\beta\overline{u_3\theta}-\tfrac{2}{3}k. \quad (16)$$

Equation (16) is approximated by assuming the stably stratified flow condition

$$\left(\frac{\partial\overline{U_3}}{\partial x_1}\approx 0, \frac{\partial\overline{U_3}}{\partial x_2}\approx 0, \frac{\partial\overline{U_3}}{\partial x_3}\approx 0\right)$$

$$-\overline{u_3^2} \simeq \frac{2}{3}C'\frac{k}{\varepsilon}P_k+\tfrac{4}{3}C'\frac{k}{\varepsilon}g_3\beta\overline{u_3\theta}-\tfrac{2}{3}k. \quad (17)$$

On the other hand, shear stress $-\overline{u_1u_3}$ is expressed as follows when applying the EVM [equation (7)]:

$$-\overline{u_1u_3} = \nu_t f_{BV}\left(\frac{\partial\overline{U_1}}{\partial x_3}+\frac{\partial\overline{U_3}}{\partial x_1}\right)\simeq \nu_t f_{BV}\frac{\partial\overline{U_1}}{\partial x_3}. \quad (18)$$

From equation (15) and (18), equation (19) is derived.

$$C'\frac{k}{\varepsilon}\overline{u_3^2}\frac{\partial\overline{U_1}}{\partial x_3} = \nu_t f_{BV}\frac{\partial\overline{U_1}}{\partial x_3}. \quad (19)$$

Then the model function f_{BV} is defined as follows with the aid of equation (17):

$$f_{BV} = \left(C'\frac{k}{\varepsilon}\overline{u_3^2}\frac{\partial\overline{U_1}}{\partial x_3}\right)\Big/\left(\nu_t\frac{\partial\overline{U_1}}{\partial x_3}\right) \quad (20)$$

$$= C_{BV1}-C_{BV2}\frac{P_k}{\varepsilon}+C_{BV3}\frac{G_k}{\varepsilon}. \quad (21)$$

The model constants are originally given by the ASM by Launder [9] as follows: $C_{BV1} = 2C'/3C_\mu = 1.63$, $C_{BV2} = 2C'^2/3C_\mu = 0.36$, $C_{BV3} = 4C'^2/3C_\mu = 0.72$. However, the value of C_{BV1} is modified to 1.36 by optimization, as shown in Section 2.3.

This model function f_{BV} damps $-\overline{u_1u_3}$, $-\overline{u_2u_3}$ where the flow is stable ($G_k < 0$). In an unstable region, equation (21) indicates that f_{BV} becomes more than 1. However, in this study f_{BV} is set to be 1 in unstable and neutral regions.

2.2. *Model function* $f_{B\theta}$ *for damping* $\overline{u_i\theta}$

$f_{B\theta}$ is the model function designed to damp the vertical turbulent heat flux $(-\overline{u_3\theta})$.

$$-\overline{u_1\theta} = \frac{\nu_t}{\sigma_\theta}\frac{\partial\overline{\Theta}}{\partial x_1} \quad (22)$$

$$-\overline{u_2\theta} = \frac{\nu_t}{\sigma_\theta}\frac{\partial\overline{\Theta}}{\partial x_2} \quad (23)$$

$$-\overline{u_3\theta} = \frac{\nu_t}{\sigma_\theta}f_{B\theta}\frac{\partial\overline{\Theta}}{\partial x_3}. \quad (24)$$

$f_{B\theta}$ is derived by approximating the turbulent heat flux transport equation (25).

$$\frac{D\overline{u_i\theta}}{Dt} = P_{i\theta(1)}+P_{i\theta(2)}+G_{i\theta}+\Phi_{i\theta}+D_{i\theta}-\varepsilon_{i\theta}. \quad (25)$$

For modeling the pressure–temperature gradient correlation term ($\Phi_{i\theta}$), IPM is used as follows:

$$\Phi_{i\theta} = -C_{i\theta1}\frac{\varepsilon}{k}\overline{u_i\theta}-C_{i\theta2}P_{i\theta(2)}-C_{i\theta3}G_{i\theta}. \quad (26)$$

By neglecting the convection and diffusion terms in equation (25), equation (27) is derived with equation (26). This is also the so-called WET model [8]. The model constants are given as $C_{\theta1} = C_{\theta2} = C_{\theta3} = 0.25$.

$$-\overline{u_i\theta}$$

$$\approx \frac{k}{\varepsilon}\left\{C_{\theta 1}\overline{u_i u_k}\frac{\partial\overline{\Theta}}{\partial x_k}+C_{\theta 2}\overline{u_k\theta}\frac{\partial\overline{U_i}}{\partial x_k}+C_{\theta 3}g_i\beta\overline{\theta^2}\right\} \tag{27}$$

$$=\frac{k}{\varepsilon}\left\{C_{\theta 1}\overline{u_i u_k}\frac{\partial\overline{\Theta}}{\partial x_k}+C_{\theta 2}\overline{u_k\theta}\frac{\partial\overline{U_i}}{\partial x_k}-C_{\theta 3}g_i\beta\frac{k}{\varepsilon}\overline{u_k\theta}\frac{\partial\overline{\Theta}}{\partial x_k}\right\}. \tag{28}$$

$\overline{\theta^2}$ in equation (27) is given by approximating the $\overline{\theta^2}$-equation as follows:

$$\frac{D\overline{\theta^2}}{Dt}=P_\theta+D_\theta-2\varepsilon_\theta. \tag{29}$$

Here local equilibrium is assumed.

$$0=P_\theta-2\varepsilon_\theta. \tag{30}$$

Furthermore, by defining R as a ratio of the time scale of temperature fluctuation to time scale of velocity fluctuation [equation (31)], P_θ and ε_θ are given as follows:

$$R=(\overline{\theta^2}/2\varepsilon_\theta)/(k/\varepsilon) \tag{31}$$

$$\varepsilon_\theta=(\overline{\theta^2}/2R)/(k/\varepsilon) \tag{32}$$

$$P_\theta=2\varepsilon_\theta=(\overline{\theta^2}/R)/(k/\varepsilon). \tag{33}$$

Thus equation (34) is given:

$$\overline{\theta^2}=-R\frac{k}{\varepsilon}P_\theta=-2R\frac{k}{\varepsilon}\overline{u_k\theta}\frac{\partial\overline{\Theta}}{\partial x_k}=-\frac{k}{\varepsilon}\overline{u_k\theta}\frac{\partial\overline{\Theta}}{\partial x_k}. \tag{34}$$

Here, the flow is assumed to be local equilibrium and R is assumed as 0.5 [10].

From equation (28), equation (35) is derived.

$$-\overline{u_3\theta}=\frac{k}{\varepsilon}\left\{C_{\theta 1}\left(\overline{u_1u_3}\frac{\partial\overline{\Theta}}{\partial x_1}+\overline{u_2u_3}\frac{\partial\overline{\Theta}}{\partial x_2}+\overline{u_3^2}\frac{\partial\overline{\Theta}}{\partial x_3}\right)\right.$$
$$+C_{\theta 2}\left(\overline{u_1\theta}\frac{\partial\overline{U_3}}{\partial x_1}+\overline{u_2\theta}\frac{\partial\overline{U_3}}{\partial x_2}+\overline{u_3\theta}\frac{\partial\overline{U_3}}{\partial x_3}\right)$$
$$\left.-C_{\theta 3}g_3\beta\frac{k}{\varepsilon}\left(\overline{u_1\theta}\frac{\partial\overline{\Theta}}{\partial x_1}+\overline{u_2\theta}\frac{\partial\overline{\Theta}}{\partial x_2}+\overline{u_3\theta}\frac{\partial\overline{\Theta}}{\partial x_3}\right)\right\}. \tag{35}$$

By assuming

$$\frac{\partial}{\partial x_3}\gg\frac{\partial}{\partial x_1}\sim\frac{\partial}{\partial x_2}$$

considering the flow condition of a stably stratified flow, equation (35) is approximated as equation (36).

$$-\overline{u_3\theta}\simeq\frac{k}{\varepsilon}\left\{C_{\theta 1}\overline{u_3^2}\frac{\partial\overline{\Theta}}{\partial x_3}-C_{\theta 3}g_3\beta\frac{k}{\varepsilon}\overline{u_3\theta}\frac{\partial\overline{\Theta}}{\partial x_3}\right\}. \tag{36}$$

From equations (17), (24) and (36), the model function $f_{B\theta}$ is derived.

$$f_{B\theta}=\left[\frac{k}{\varepsilon}\left\{C_{\theta 1}\overline{u_3^2}\frac{\partial\overline{\Theta}}{\partial x_3}-C_{\theta 3}g_3\beta\frac{k}{\varepsilon}\overline{u_3\theta}\frac{\partial\overline{\Theta}}{\partial x_3}\right\}\right]\Big/\left[\frac{\nu_t}{\sigma_\theta}\frac{\partial\overline{\Theta}}{\partial x_3}\right] \tag{37}$$

$$=C_{B\theta 1}-C_{B\theta 2}\frac{P_k}{\varepsilon}+C_{B\theta 3}\frac{G_k}{\varepsilon}. \tag{38}$$

The model constants are originally given from the ASM [9] as follows. $C_{B\theta 1}=2C_{\theta 1}\sigma_\theta/3C_\mu=1.67$, $C_{B\theta 2}=2C_{\theta 1}C'\sigma_\theta/3C_\mu=0.37$, $C_{B\theta 3}=\sigma_\theta(C_{\theta 1}C'/3+C_{\theta 3})/C_\mu=3.2$. However, the values of $C_{B\theta 1}$ and $C_{B\theta 3}$ are modified by optimization, as shown in Section 2.3; $C_{B\theta 1}=1.37$, $C_{B\theta 3}=1.6$.

This model function $f_{B\theta}$ damps where the flow is stable ($G_k<0$). In unstable or neutral conditions ($G_k\geqslant 0$), $f_{B\theta}$ is set to be 1 in this study.

2.3. *Setting of model constants*

When there is no buoyancy force, the model functions are expressed simply

$$f_{BV}=C_{BV1}-C_{BV2}\frac{P_k}{\varepsilon} \tag{39}$$

$$f_{B\theta}=C_{B\theta 1}-C_{B\theta 2}\frac{P_k}{\varepsilon}. \tag{40}$$

C_{BV1}, C_{BV2}, $C_{B\theta 1}$, $C_{B\theta 2}$ are defined so as to satisfy $f_{BV}=f_{B\theta}=1$, when the local equilibrium, $P_k=\varepsilon$, can be assumed. Thus

$$C_{BV1}=1+C_{BV2} \tag{41}$$

$$C_{B\theta 1}=1+C_{B\theta 2}. \tag{42}$$

C_{BV1} and $C_{B\theta 1}$ are modified to 1.36 and 1.37 using equations (41) and (42). In the $\overline{u_i\theta}$ equation [equation (27)], $\overline{\theta^2}$ works to transport heat against the stratification when the flow is stably stratified, because $\overline{\theta^2}$ is always positive. Thus, this leads to the reduction of the downward heat transport of $\overline{u_3\theta}$. It sometimes leads the calculation to diverge. It is reported that the WET model with the condition of local equilibrium of $\overline{\theta^2}$ [equation (28)] did not always lead to a stationary solution when it was applied to a stably stratified flow [11]. In the stably stratified region, the local equilibrium assumption usually over-estimates $\overline{\theta^2}$. In this case, $|\overline{u_3\theta}|$ becomes smaller, as stated above, thus $f_{B\theta}$ works to over damp. To overcome this difficulty, we set the value of $C_{B\theta 3}$ to be smaller than the value given by the ASM.

2.4. *Behavior of damping functions* f_{BV} *and* $f_{B\theta}$

2.4.1. *Behavior of damping functions by* P_k/ε *(when there is little effect from buoyancy).* Hossain and Rodi reported on the relationship between P_k/ε and the turbulence model constant $\tilde{C}_\mu$ based on experimental results [12]. Viollet derived the next relation by ASM approximation [13]:

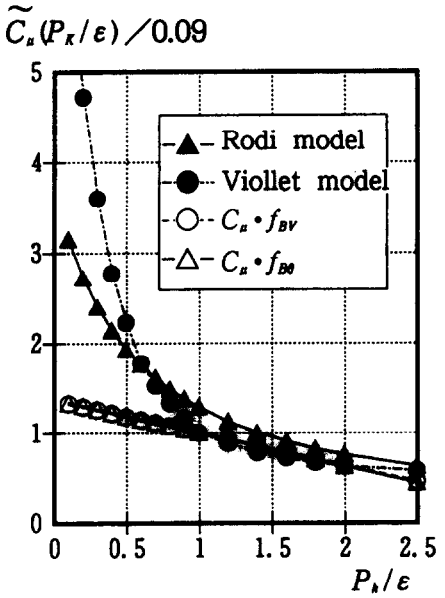

Fig. 1. Change of $\tilde{C}_\mu$ by P_k/ε.

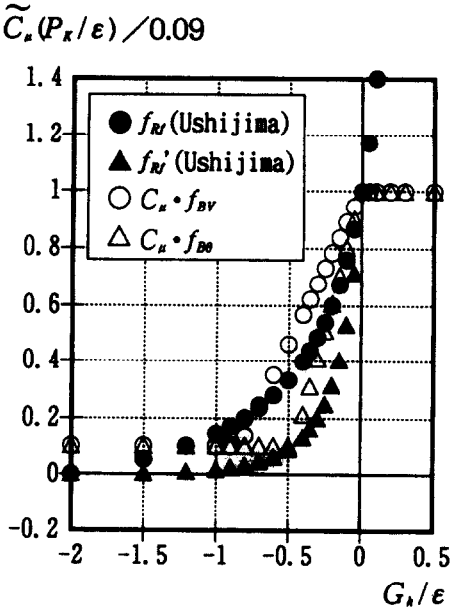

Fig. 2. Change of $\tilde{C}_\mu$ by G_k/ε.

$$\tilde{C}_\mu(P_k/\varepsilon) = \tfrac{2}{3}(1-C_2)\frac{C_1-1+C_2\dfrac{P_k}{\varepsilon}}{\left(C_1-1+\dfrac{P_k}{\varepsilon}\right)^2}. \tag{43}$$

Here, $\tilde{}$ is added to C_μ to differentiate it from the constant $C_\mu(=0.09)$. In the case of the new model proposed here, $\tilde{C}_\mu(P_k/\varepsilon)$ corresponds to $C_\mu f_{BV}$ or $C_\mu f_{B\theta}$.

Figure 1 shows the change of $\tilde{C}_\mu$ by P_k/ε for various models. Here G_k is assumed to be negligible. In the region where P_k/ε is more than 1, i.e. in the region with high turbulence generation by mean shear, all models agree well with each other. However, in the weak shear region, $P_k/\varepsilon < 1$, the proposed models show the most moderate change among them. The model including f_{BV} and $f_{B\theta}$ shows smaller values of $\tilde{C}_\mu$ than the values given by the models of Rodi or Viollet.

2.4.2. *Behavior of damping functions by* G_k/ε. Ushijima *et al.* investigated the relationship between the turbulence quantities and the bulk Richardson number R_i [cf. equation (58)] in a two-dimensional thermally stratified open channel flow, and proposed a model for revising the EVM expression optimized by their experimental results [6]

$$-\overline{u_1u_3} = C_\mu f_{Rf}\frac{k^2}{\varepsilon}\left(\frac{\partial\overline{U_1}}{\partial x_3}+\frac{\partial\overline{U_3}}{\partial x_1}\right) \tag{44}$$

$$-\overline{u_3\theta} = \frac{C_\mu}{\sigma_\theta}f_{Rf}\frac{k^2}{\varepsilon}\frac{\partial\overline{\Theta}}{\partial x_3} \tag{45}$$

$$f_{Rf} = \frac{1-1.5R_f}{1+1.5R_f} \tag{46}$$

$$f_{Rf} = \frac{1-1.5R_f}{1+1.5R_f}\frac{1-1.5R_f}{1+2.6R_f}. \tag{47}$$

Here, R_f: flux Richardson number, $-G_k/P_k$. In equations (46) and (47), R_i is replaced by R_f ($R_f = R_i/\sigma_\theta$; in this case, σ_θ is assumed to be constant, $\sigma_\theta = 1$).

If the local equilibrium, $P_k + G_k \fallingdotseq \varepsilon$, is assumed and f_{Rf}, f'_{Rf} become simple, as shown below.

$$f_{Rf} = \frac{1+1.5G_k/P_k}{1-1.5G_k/P_k} \fallingdotseq \frac{\varepsilon-G_k+1.5G_k}{\varepsilon-G_k-1.5G_k} = \frac{1+0.5G_k/\varepsilon}{1-2.5G_k/\varepsilon} \tag{48}$$

$$f'_{Rf} \fallingdotseq \frac{(1+0.5G_k/\varepsilon)^2}{(1-2.5G_k/\varepsilon)\cdot(1-3.6G_k/\varepsilon)}. \tag{49}$$

The expression of f_{BV}, $f_{B\theta}$ proposed here also becomes simple when $P_k+G_k \fallingdotseq \varepsilon$ is assumed.

$$f_{BV} \fallingdotseq C_{BV1} - C_{BV2}\frac{\varepsilon-G_k}{\varepsilon} + C_{BV3}\frac{G_k}{\varepsilon}$$

$$= 1.0 + 1.08\frac{G_k}{\varepsilon} \tag{50}$$

$$f_{B\theta} \fallingdotseq 1.0 + 1.97\frac{G_k}{\varepsilon}. \tag{51}$$

These model functions show similar changes by G_k/ε as shown in Fig. 2. Compared with the model of Ushijima *et al.* [6], the proposed model has the following advantages:

(1) The model proposed by Ushijima *et al.* [6] is not easily applied when the main flow is not defined, since it uses the bulk Richardson number [equation (58)]. However, the proposed model is designed to be applied to any three-dimensional flowfields.

(2) Ushijima *et al.* [6] derived their model empirically based on experimental data. However, the proposed model is based on transport equations of $\overline{u_\mu u_j}$ and $\overline{u_i\theta}$.

3. DEVELOPMENT OF A NEW LOW-REYNOLDS NUMBER k–ε MODEL WHICH IS APPLICABLE TO A LAMINAR REGION AWAY FROM THE WALL

When the flow is highly stably stratified, the turbulence intensity decreases and thereby, the flow becomes pseudo-laminar. This phenomenon is observed not only in the vicinity of the wall, but also in areas away from the wall.

Since Jones and Launder proposed the low-Reynolds-number k–ε model, various types of the model have been proposed [14]. However, almost all previous models are optimized to handle the so-called low-Reynolds-number effect due to wall echo, which is the inviscid characteristics of fluid motion. The turbulence velocity fluctuation and the flux in the normal direction to the wall decreases because of the wall reflection effect of the fluctuating pressure. They do not consider the low-Reynolds-number effect away from the wall to be caused by thermal stratification, etc. A new low-Reynolds-number k–ε model which is applicable in both regions is needed for the application to room air flows. Thus a new low-Reynolds-number k–ε model is proposed here.

Recently, Abe *et al.* proposed a new low-Reynolds-number k–ε model [15], which is applicable to a flowfield including separation and reattachment. In their model, the parameters of the model function f_μ are defined by y^* $(=u_\varepsilon y/\nu = y/\eta$, here $u_\varepsilon = (\nu/\varepsilon)^{1/4}$; Kolmogorov velocity scale, and $\eta = (\nu^3/\varepsilon)^{1/4}$; Kolmogorov length scale). This model succeeds in simulating a separated flowfield with a backward facing step.

The Abe–Nagano model is shown as follows [15]:

$$f_\mu = \left\{1-\exp\left(-\frac{y^*}{14}\right)\right\}^2 \times\left[1+\left(\frac{5}{Rt^{3/4}}\right)\exp\left\{-\left(\frac{Rt}{200}\right)^2\right\}\right]. \quad (52)$$

3.1. *Modification of model function* f_μ

A new model function f_μ, based on the Abe–Nagano model, is given as follows. In the new model, model function is determined by not only y^*, but also $Rt(=k^2/(\nu\varepsilon) = l/\eta, l = k^{3/2}/\varepsilon)$.

$$f_\mu = \underbrace{\left\{1-\exp\left(-\frac{y^*}{14}\right)\right\}}_{(A)} \underbrace{\left\{1-\exp\left(-\frac{Rt^{3/4}}{2.4}\right)\right\}}_{(B)} \times \underbrace{\left\{1+\left(\frac{1.5}{Rt^{5/4}}\right)\right\}}_{(C)}. \quad (53)$$

Terms (A), (B), (C) in equation (53) have the following roles:

(A) Van Driest type damping function of ν_t from the buffer to log-law region by y^*. Near-wall damping function.

(B) Non-near-wall damping function of ν_t by Rt. Term (B) reflects the phenomenon of laminarization in the area away from the wall. In the near-wall region, term (B) works the same way as term (A).

(C) Term for satisfying the limiting behavior of wall turbulence.

The model function f_μ is required to reproduce the near-wall limiting behavior $f_\mu \propto y^{-1}$. The new model function here satisfies this limiting behavior.

3.2. *Model function* f_2 *in* ε*-equation*

f_2 is given as in the Abe–Nagano model [15]

$$f_2 = \left\{1-\exp\left(-\frac{y^*}{3.1}\right)\right\}^2\left[1-0.3\exp\left\{-\left(\frac{Rt}{6.5}\right)^2\right\}\right]. \quad (54)$$

4. ASSESSMENT OF THE NEW LOW-REYNOLDS-NUMBER k–ε MODEL IN THERMAL CAVITY FLOW

4.1. *Specification of thermal cavity flow used* (Fig. 3)

To examine the performance of the proposed low-Reynolds-number k–ε model, it is applied to a flow in which the laminarization phenomenon is observed away from the wall. Figure 3 shows a schematic view of the thermal cavity flow [16]. The flow is driven by the temperature difference between the hot wall (68.0°C) and the cold wall (22.2°C). It is laminarized not only in the vicinity of the wall, but also away from the wall.

4.2. *Boundary conditions at the wall surface* (Fig. 3)

No slip boundary condition is used.

4.3. *Basic equations and model functions*

$$(k-eq)\frac{Dk}{Dt} = \frac{\partial}{\partial x_j}\left\{\left(\nu+\frac{\nu_t}{\sigma_k}\right)\frac{\partial k}{\partial x_j}\right\}+P_k+G_k-\varepsilon \quad (55)$$

$$(\varepsilon-eq)\frac{D\varepsilon}{Dt} = \frac{\partial}{\partial x_j}\left\{\left(\nu+\frac{\nu_t}{\sigma_\varepsilon}\right)\frac{\partial \varepsilon}{\partial x_j}\right\} + \frac{\varepsilon}{k}(C_{\varepsilon 1}f_1 P_k + C_{\varepsilon 3}f_1 G_k - C_{\varepsilon 2}f_2\varepsilon) \quad (56)$$

$$\nu_t = C_\mu f_\mu \frac{k^2}{\varepsilon}. \quad (57)$$

f_μ and f_2 are given as defined in equations (53) and (54). $f_1 = 1.0$. $C_{\varepsilon 1} = C_{\varepsilon 3} = 1.5$, $C_{\varepsilon 2} = 1.9$, $C_\mu = 0.09$, $\sigma_k = 1.4$, $\sigma_\varepsilon = 1.4$.

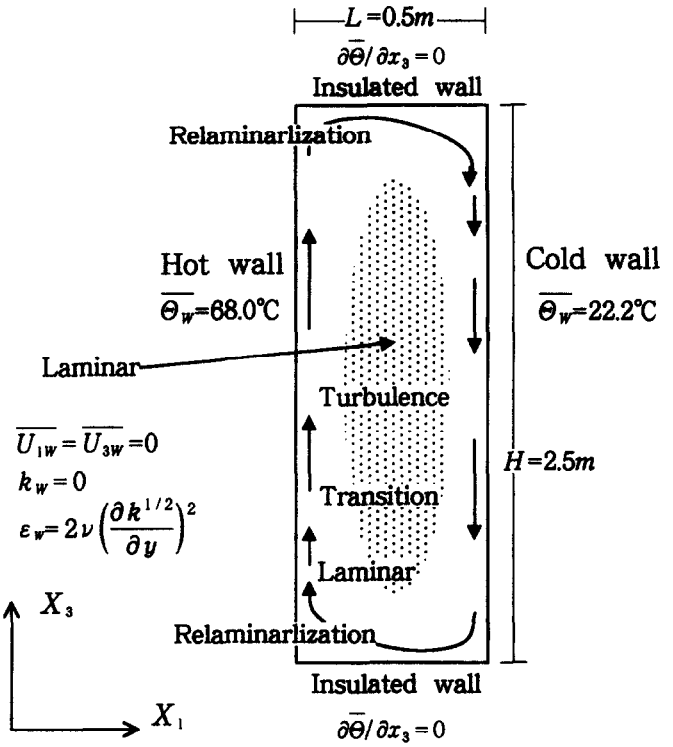

Fig. 3. Thermal cavity used.

The results given by the proposed model are compared with the results by the Launder–Sharma model [17] and the Abe–Nagano model [15].

In this calculation, the model functions f_{BV}, $f_{B\theta}$ for the thermal damping are not included, because a large circulation is produced along the walls and the buoyancy damping is not so strong.

4.4. *Grids and schemes for calculation*

The computational domain is discretized into $(50+2)(x_1) \times (100+2)(x_3)$. The staggered grid system is used. The convection terms of momentum equations were approximated by means of the QUICK scheme, and those for scalar equations were approximated by means of the upwind scheme. The SIMPLE algorithm is used for pressure relaxation.

4.5. *Results and discussion*

Figures 4–6 show the results of the mean velocity profile, temperature profile and k profile, respectively.

The Abe–Nagano model [15] reproduces the velocity profile well; however, it does not reproduce the profile of k accurately enough at the area away from the wall (Fig. 6, at $X_1 = 0.1$ or 0.4). On the other hand, the Launder–Sharma model can reproduce the k profile well; however, it cannot reproduce the velocity profile with high accuracy. The present model shows the best agreement. Therefore, it may be concluded that the low-Reynolds-number treatment defined here can reproduce the low-Reynolds-number effect, both for near wall region and away from the wall.

In the experiment, it is reported that there was some heat loss due to insufficient thermal insulation. Thus, the temperature profile from the experiment was lower than the results given from the computations.

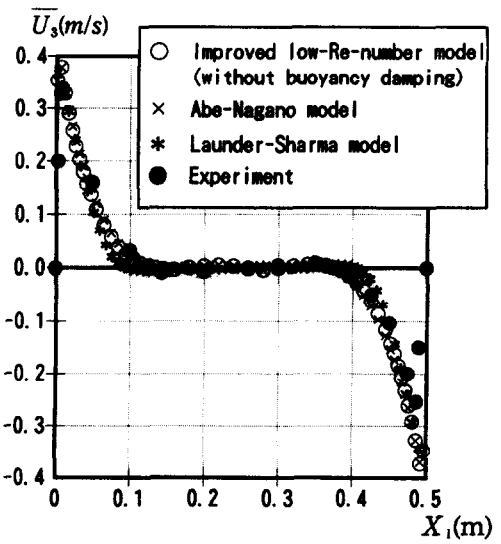

Fig. 4. Profile of $\overline{U_3}$ (horizontal center line, $X_3 = 0.5$ H).

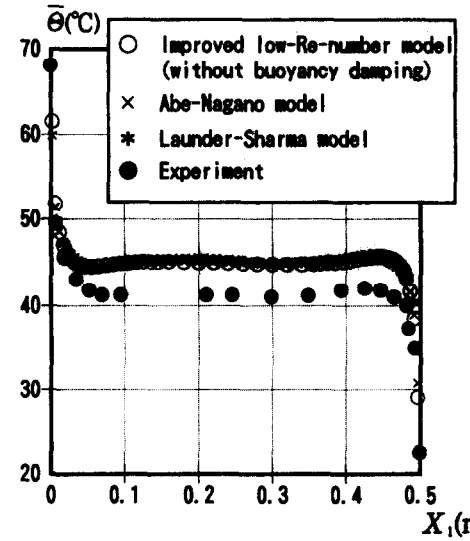

Fig. 5. Profile of $\overline{\Theta}$ (horizontal center line, $X_3 = 0.5$ H).

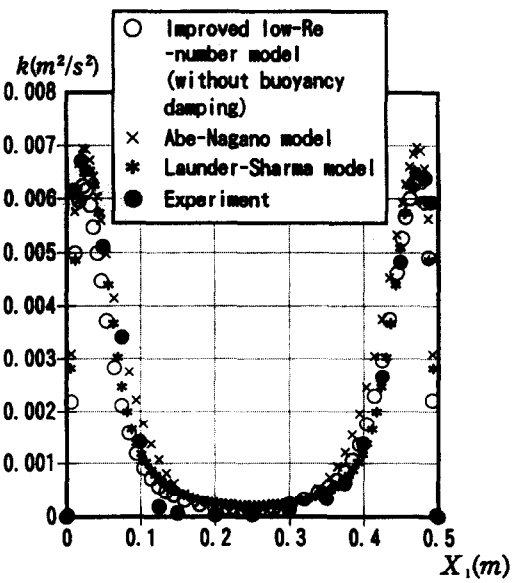

Fig. 6. Profile of k (horizontal center line, $X_3 = 0.5$ H).

5. ASSESSMENT OF IMPROVED k–ε EVM WITH STABLY STRATIFIED SHEAR FLOW WITHIN A TWO-DIMENSIONAL CHANNEL

5.1. *Specification of the stably stratified channel flow used*

Figure 7 shows a schematic view of the stably stratified open channel flow. The experiment was conducted by Ushijima *et al.* [6].

5.2. *Boundary conditions*

(1) *Inflow boundary.* The measured results were used for the inlet boundary conditions of mean velocity, mean temperature, turbulence energy k and dissipation rate ε. The mean velocity of warm water ($\overline{U_h}$) is 0.072 m s^{-1} and the mean temperature of warm water ($\overline{\Theta_h}$) is 29.2°C. The mean velocity of cold water ($\overline{U_c}$) is 0.118 m s^{-1} and the mean temperature of cold water ($\overline{\Theta_c}$) is 14.5°C. In this case, the bulk Richardson number R_i is given as follows:

$$R_i = -g_3\beta(\overline{\Theta_h} - \overline{\Theta_c})h/(\overline{U_h} - \overline{U_c})^2 = 4.6. \quad (58)$$

(2) *Outlet boundary.* Free slip.

(3) *Surface boundary of the open water channel.* The fluctuation of the water surface is very small, so the surface of the open channel flow is assumed to be fixed and the free slip boundary condition is adopted.

(4) *Wall boundary of the channel bottom.* The wall function of the generalized log-law is used.

5.3. *Basic equations and model functions*

Equations (55)–(57) are used. $\overline{u_i u_j}$, $\overline{u_i\theta}$ are modeled by equations (3)–(8) and (22)–(24). Thus, the improved k–ε model including f_{BV} [equation (21)] and $f_{B\theta}$ [equation (38)] is used here (cf. note). To avoid negative diffusion, $f_{BV}, f_{B\theta} \geqslant 0.1$ is imposed. The flow field is very turbulent, so the low-Reynolds-number effect is negligible in this case.

$$f_\mu = f_1 = f_2 = 1.0, \quad C_{\varepsilon 1} = C_{\varepsilon 3} = 1.5, \quad C_{\varepsilon 2} = 1.9,$$

$$C_\mu = 0.09, \quad \sigma_k = 1.4, \quad \sigma_\varepsilon = 1.4.$$

The results given by the proposed model are compared with the results given by the standard k–ε model, which does not include f_{BV} and $f_{B\theta}$.

5.4. *Grids and schemes for calculation*

The computational domain is discretized into $(75+2)(x_1) \times (28+2)(x_3)$ (cf. Fig. 7). The domain is discretized equally in each direction. The convective terms are approximated by means of the QUICK scheme. The other numerical methods are identical with those used in the case of thermal cavity flow.

5.5. *Results and discussion*

Figure 8 shows the results of the mean velocity vectors, and Fig. 9 shows the results of temperature distribution. Figure 9(a) illustrates the results given by the proposed model which includes the damping function f_{BV} and $f_{B\theta}$.

Figure 9(b) shows the results given by the standard k–ε model.

The hot water in the upper region and the cold water in the lower region are mixed gradually. The thickness of the mixing layer given by the improved model is smaller than that given by the standard k–ε model.

Figure 10 shows the profile of mean streamwise velocity ($\overline{U_1}$) at 1.0 m downstream from the inlet. Figure 11 shows the profile of mean temperature at the same position.

The results given by the proposed model are clearly better than the ones given by the standard k–ε model. The standard k–ε model does not reproduce well the damping effect on vertical heat and momentum transports by the stable stratification. However, the pro-

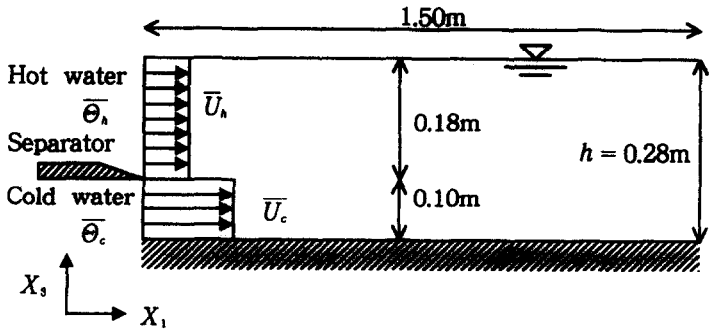

Fig. 7. Stably stratified open channel.

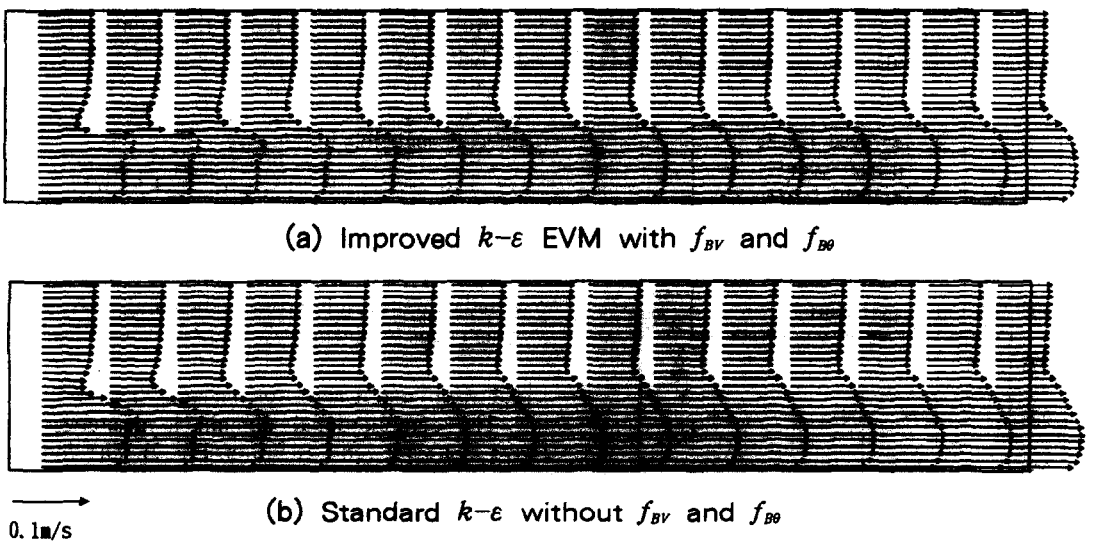

Fig. 8. Velocity distribution, (a) improved k–ε EVM with f_{BV} and $f_{B\theta}$, (b) standard k–ε without f_{BV} and $f_{B\theta}$.

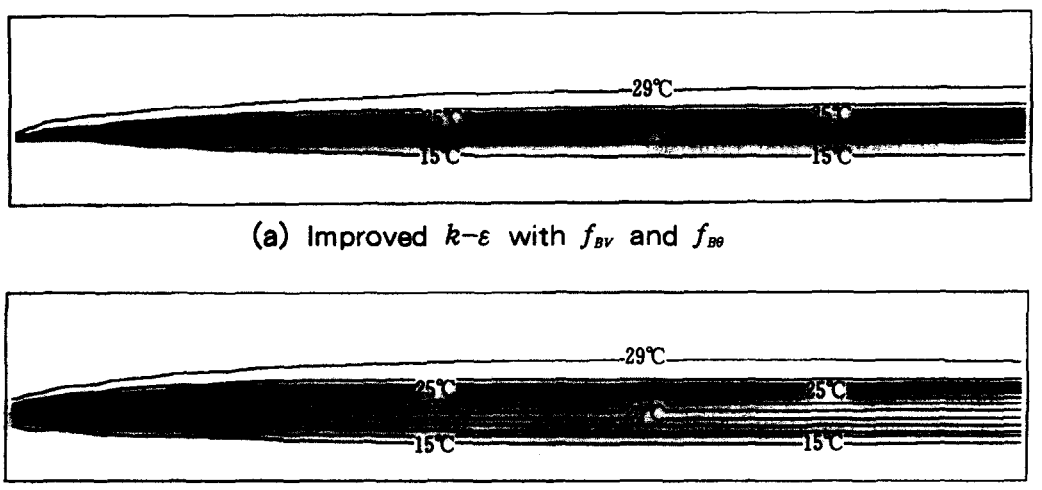

Fig. 9. Temperature distribution, (a) improved k–ε with f_{BV} and $f_{B\theta}$, (b) standard k–ε without f_{BV} and $f_{B\theta}$.

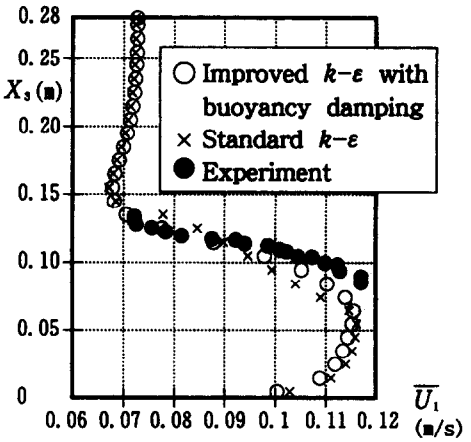

Fig. 10. Comparison of $\overline{U_1}$ profile.

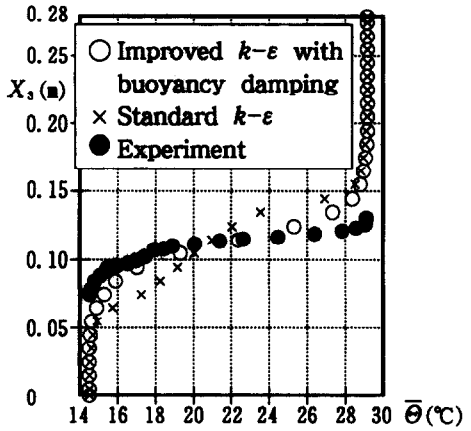

Fig. 11. Comparison of $\overline{\Theta}$ profile.

posed model can predict this effect well. When f_{BV} and $f_{B\theta}$ are incorporated into the EVM of $\overline{u_iu_j}$ and $\overline{u_i\theta}$, the thickness of the mixing layer becomes smaller and the results become more accurate.

Since there exists slight, but clear, differences between the results of the experiment and the simulation, there should be some room for improvement of this proposed model. However, the model has achieved considerable improvement and it would require many additional terms which are included in DSM to obtain more accurate results.

6. APPLICATION OF THE IMPROVED k–ε EVM TO STABLY STRATIFIED AND LOW-REYNOLDS-NUMBER FLOW FIELD IN AN ENCLOSURE WITH SUPPLY AND EXHAUST

6.1. *Specification of room model used*

Figure 12 shows a schematic view of the two-dimensional room model with supply and exhaust [18]. The ceiling is heated, thus the flowfield is stably stratified.

6.2. *Boundary condition* (Fig. 12)

(1) *Supply boundary condition.* The inflow boundary conditions for mean velocity, mean temperature and turbulence energy k_{in} of the supply jet are given by the experimental data. The ε_{in} is given as follows:

$$\varepsilon_{in} = C_\mu k_{in}^{3/2}/(0.5\, l_{in}).$$

(2) *Exhaust boundary condition.* The exhaust mean velocity is given by the experimental data. Other quantities are given by the free slip condition.

(3) *Wall boundary condition.* The velocity and k_{wall} are given based on the non-slip condition. The wall temperature is given by the experimental data. The ε_{wall} is given as follows:

$$\varepsilon_{wall} = 2\nu(\partial k^{1/2}/\partial y)^2.$$

6.3. *Basic equations and model functions*

Equations (55)–(57) are used. In this case study, the effects of both the buoyancy damping ($f_{BV}, f_{B\theta}$) and the laminarization (f_μ) are included in the k–ε model (cf. note).

$\overline{u_iu_j}$, $\overline{u_i\theta}$ are modeled by equations (3)–(8) and (22)–(24). f_μ and f_2 are defined as equations (53) and (54). $f_1 = 1.0$. To avoid negative diffusion, $f_{BV}, f_{B\theta} \geqslant 0.1$ is imposed.

$$C_{\varepsilon 1} = C_{\varepsilon 3} = 1.5, \quad C_{\varepsilon 2} = 1.9, \quad C_\mu = 0.09,$$
$$\sigma_k = 1.4, \quad \sigma_\varepsilon = 1.4.$$

6.4. *Grids and schemes for calculation*

The computational domain is discretized into $(100+2)(x_1) \times (100+2)(x_3)$. The numerical method is the same one as used in the previous calculations.

6.5. *Results and discussion*

The results given from the improved k–ε EVM with f_μ [equation (53)] and $f_{BV}, f_{B\theta}$ [equations (21) and (38)] and the results given from the low-Reynolds-number k–ε model without $f_{BV}, f_{B\theta}$ are compared.

Figure 13(a) shows the result of the mean velocity vectors given by the improved model with $f_{BV}, f_{B\theta}$, and Fig. 13(b) shows those given by the low-Reynolds-number k–ε model without $f_{BV}, f_{B\theta}$. Figure 14 shows the temperature distribution given by the improved model with $f_{BV}, f_{B\theta}$, and Fig. 15 shows the distribution of damping function f_{BV}.

In the results of the low-Reynolds-number model without $f_{BV}, f_{B\theta}$ [Fig. 13(b)], the flow along the diagonal line from the right bottom corner to the left top corner is not straight. This flow pattern is not correct compared with the results of the experiment. In the improved model with damping function f_μ, f_{BV} and $f_{B\theta}$, the flow along the diagonal line is revised and shows a straight line. Flow visualization by the experiment shows the straight flow along the diagonal line, and the improved model reproduces the experiment accurately. Laurence and Craft are trying to simulate this flow using the differential stress model. Their result is similar to the result given by the improved model.

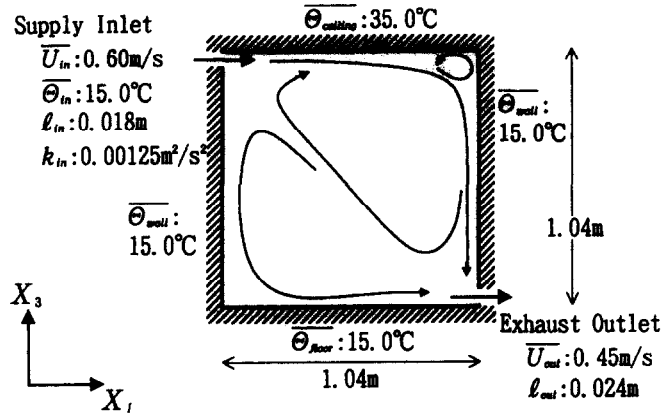

Fig. 12. Two-dimensional enclosed space with supply and exhaust (non-isothermal flow field).

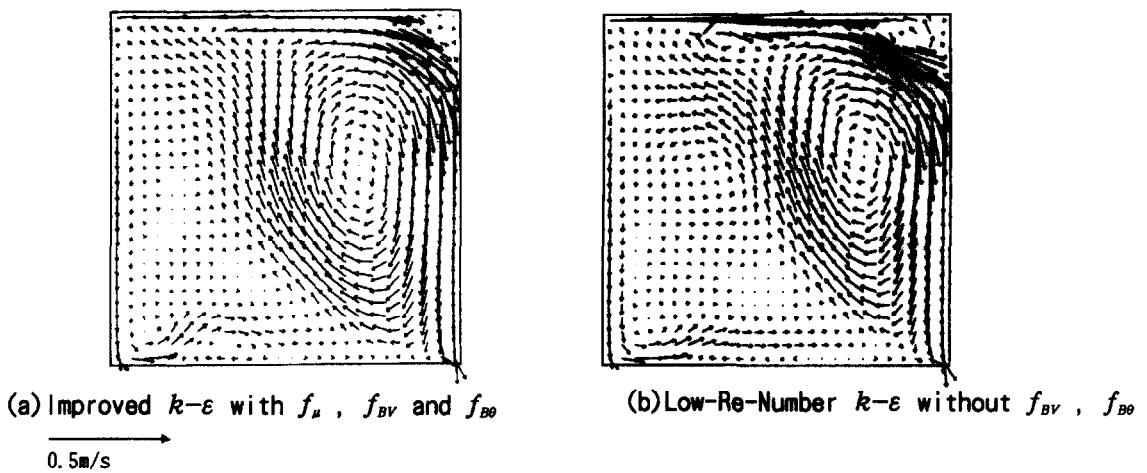

Fig. 13. Velocity distribution, (a) improved k–ε with f_μ, f_{BV} and $f_{B\theta}$, (b) low-Re-number k–ε without f_{BV}, $f_{B\theta}$.

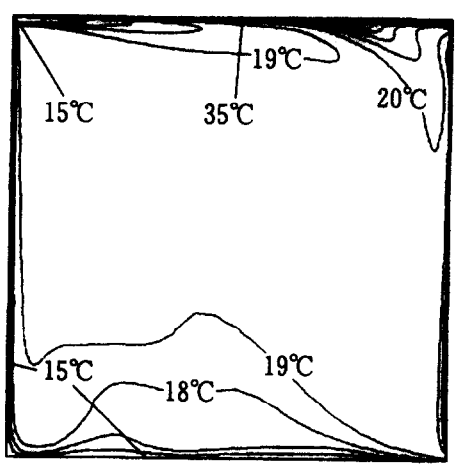

Fig. 14. Temperature distribution (improved k–ε with f_μ, f_{BV} and $f_{B\theta}$).

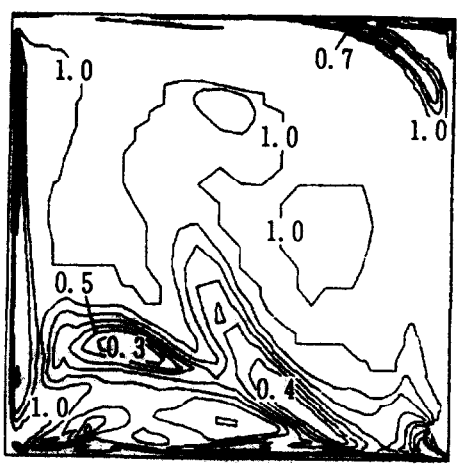

Fig. 15. Distribution of f_{BV} (improved k–ε with f_μ, f_{BV} and $f_{B\theta}$).

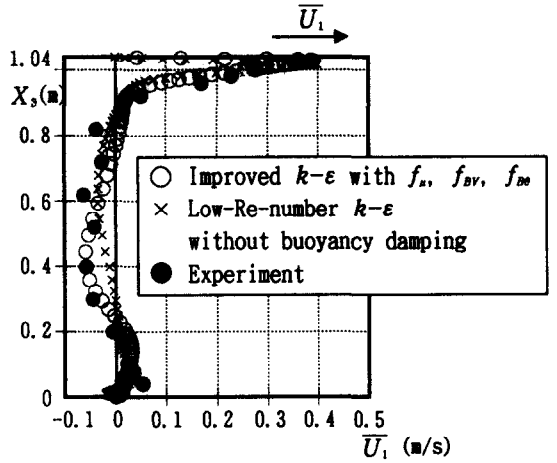

Fig. 16. Comparison of $\overline{U_1}$ profile (vertical center line; $X_1 = 0.52$).

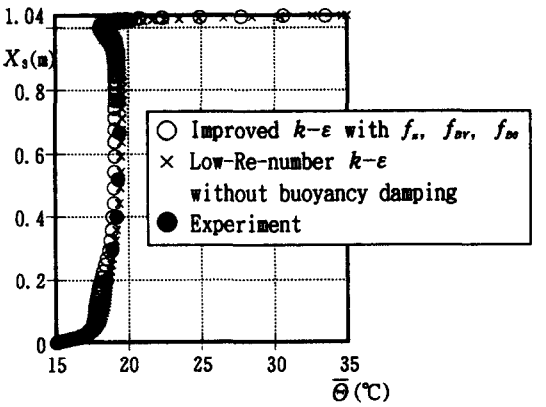

Fig. 18. Comparison of $\overline{\Theta}$ profile (vertical center line; $X_1 = 0.52$).

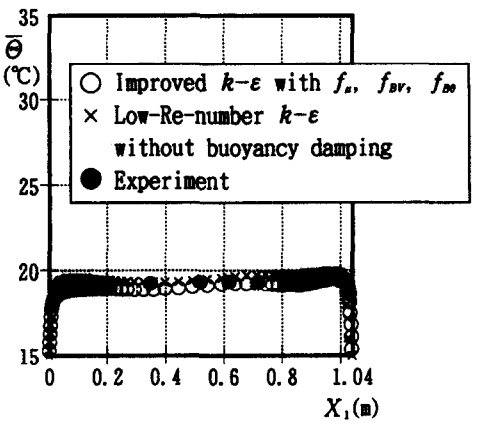

Fig. 19. Comparison of $\overline{\Theta}$ profile (horizontal center line; $X_3 = 0.52$).

In the low-Reynolds-number k–ε model without f_{BV}, $f_{B\theta}$, the position of the center of the primary vortex is located at the upper part of the cavity; however, in the improved model with damping functions f_μ, f_{BV} and $f_{B\theta}$, the position of the center stays in the lower part of the cavity. f_{BV} and $f_{B\theta}$ work well and thus, the flow at the left bottom corner becomes laminar. In the right top corner, a second vortex is observed.

Near the flow, the main stream moves from left to right; however there is a small reverse flow which goes from right to left just near the flow. Thus, a small bump is observed near the left corner on the floor.

Figure 16 shows the profile of $\overline{U_1}$ at $X_1 = 0.52$ m line (vertical center section). Figure 17 shows the profile of $\overline{U_3}$ at $X_3 = 0.52$ m line (horizontal center section). As far as the $\overline{U_1}$ profile is concerned, the results of both the improved low-Reynolds-number model without buoyancy damping and the improved model with f_μ, f_{BV} and $f_{B\theta}$ do not follow the experiment accurately. However, the proposed model with f_μ, f_{BV} and $f_{B\theta}$ predict the $\overline{U_3}$ profile much better than does the model without f_{BV}, $f_{B\theta}$.

Figure 18 shows the profile of $\overline{\Theta}$ at $X_1 = 0.52$ m line (vertical center section). Figure 19 shows the profile of $\overline{\Theta}$ at $X_3 = 0.52$ m line (horizontal center section). Computations both with and without buoyancy damping predict the temperature profiles well.

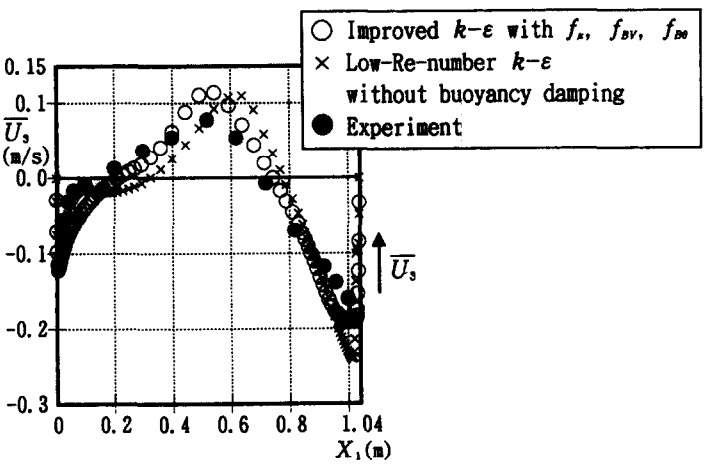

Fig. 17. Comparison of $\overline{U_3}$ profile (horizontal center line; $X_3 = 0.52$).

As mentioned before, the model introduced in this study can reproduce the buoyancy damping mechanism in the quite simple way. Though there are some discrepancies between the experiment and the simulation, these are not so large, and the model will be useful for practical use.

7. CONCLUDING REMARKS

The improved low-Reynolds-number k–ε EVM which includes the damping effect of vertical transport of heat and momentum is proposed. The model functions proposed are expressed by f_μ, f_{BV} and $f_{B\theta}$, respectively.

The new low-Reynolds-number treatment f_μ proposed here can deal with laminarization of both near-wall and non-near-wall (away from the wall).

With this non-near-wall and near-wall type low-Reynolds-number treatment (f_μ), and with the damping function of the vertical heat and momentum transport (f_{BV} and $f_{B\theta}$), three types of flow fields with stable stratification and laminarization are analyzed. The results given by the proposed k–ε EVM (with damping functions f_μ, f_{BV} and $f_{B\theta}$) are remarkable improvements over the results given from the standard k–ε model.

Note. It is possible to develop the damping functions f_{Bk}, $f_{B\varepsilon}$ for the turbulent diffusion term of k and ε equations following the derivation of f_{BV}, $f_{B\theta}$. However, they are not considered here since the effects by f_{Bk}, $f_{B\varepsilon}$ are small in the flowfields which are analyzed in this paper.

Acknowledgments—When developing the model, we had useful advice from Professor Y. Nagano (Nagoya Technical University, Japan). We were also given valuable data on their stratified channel flow experiment by Dr N. Tanaka (Central Research Institute of the Electric Power Industry, CRIEPI) and Dr S. Ushijima (CRIEPI). Numerical calculation is assisted by Mr N. Ohira (Tokyo Gas Co. Ltd). We would like to express our great gratitude to all of them.

REFERENCES

1. B. E. Launder and D. B. Spalding, The numerical computation of turbulent flows, *Comput. Meth. Appl. Mech. Engng* **3,** 269–289 (1974).
2. S. Murakami, S. Kato and R. Ooka, Comparison of numerical predictions of horizontal non-isothermal jet in room with three turbulence models k-ε, ASM and DSM, *ASHRAE Trans.* **100,** 1 (1994).
3. W. P. Jones and B. E. Launder, The calculation of low-Reynolds-number phenomenon with a two-equation model of turbulence, *Int. J. Heat Mass Transfer*, **15,** 301–314 (1972).
4. B. E. Launder, On the effect of a gravitational field on the turbulent transport of heat and momentum, *J. Fluid Mech.* **67,** 569–581 (1975).
5. K. Sagara, On the calculation of turbulent flow under gravitational influence, *Trans. Architect. Inst. Jap.* **305,** 88–96 (in Japanese) (1981).
6. S. Ushijima, N. Tanaka and S. Moriya, Improved k-ε model in stratified flows, *Preprints of 32th Symp. of Hydraulics*, pp. 655–660 (in Japanese) (1988).
7. M. Yamakawa, Ph.D. thesis at University of Tokyo (in Japanese) (1991).
8. B. E. Launder, On the computation of convective heat transfer in complex turbulent flows, *J. Heat Transfer* **110,** 1112–1128 (1988).
9. B. E. Launder, Second-moment closure: methodology and practice, UMIST Report no. TFD/82/4 (1983).
10. M. M. Gibson and B. E. Launder, Ground effects on pressure fluctuations in the atmospheric boundary layer, *J. Fluid Mech.* **86,** 491–511 (1978).
11. S. Murakami, S. Kato and S. Nagano, Study on buoyancy effected room airflow by k-ε model simulation with local equilibrium type WET heat flux modeling, *Seisan-Kenkyu*, **43,** 57–60 (in Japanese) (1990).
12. M. S. Hossain and W. Rodi, A turbulence model for buoyant flows and its application to vertical buoyant jets and plumes. In *Turbulent Buoyant Jets and Plumes* (Edited by W. Rodi), HMT-Series, Vol. 6. Pergamon Press, Oxford (1982).
13. P. L. Viollet, The modelling of turbulent recirculating flows for the purpose reactor thermal-hydraulic analysis, *Nuclear Engng Des.* **99,** 365–377 (1987).
14. V. C. Patel, W. Rodi and G. Scheuerer, Turbulence models for near-wall and low-Reynolds-number flows: a review, *AIAA J.* **23,** 1308–1319 (1984).
15. K. Abe, Y. Nagano and T. Kondo, Numerical prediction of separating and reattaching flows with a modified low-Reynolds-number k-ε model, *J. Wind Engng* Vol. 52 (1*st Int. Symp. of Computer Wind Engineering*, Tokyo), pp. 213–218 (1992).
16. R. Cheesewright, K. J. King and S. Ziai, Experimental data for the validation of computer codes for the prediction of two-dimensional buoyancy cavity flows, *Winter Annual Meeting*, ASME, HTD Vol. 60, pp. 75–81 (1986).
17. B. E. Launder and B. I. Sharma, Application of the energy-dissipation model of turbulence to the calculation of flow near a spinning disc, *Lett. Heat Mass Transfer*, **1,** 131–138 (1974).
18. D. Blay, S. Mergui and C. Niculae, Confined turbulent mixed convection in the presence of a horizontal buoyant wall jet, *Fundamentals of Mixed Convection*, HTD Vol. 213. ASME (1992).